metals

MDPI

Article

The Influence of Cerium on Inclusions, Microstructure, and Mechanical Properties of Industrial BT700L Steel

Chao Shi [1,2,3], Xiaofeng Zhang [2,3,*], Changqiao Yang [1], Jianzhong He [2,3], Peng Liu [1] and Jichun Yang [1,*]

[1] School of Rare Earth Industry, Inner Mongolia University of Science and Technology, Baotou 014010, China; 18686150286@163.com (C.S.); yangchangqiao@imust.edu.cn (C.Y.); liupeng19970210@126.com (P.L.)
[2] Technical Center of Inner Mongolia Baotou Steel Union Co., Ltd., Baotou 014010, China; hjzhong@sina.com
[3] Inner Mongolia Key Laboratory of Rare Earth Steel Products Research and Development, Baotou 014010, China
* Correspondence: zxf2015@outlook.com (X.Z.); yangjichun1963@163.com (J.Y.)

Abstract

This industrial-scale study investigates cerium's effect on inclusions, microstructure, and mechanical properties in Ti-bearing high-strength steel BT700L through comparative trials of two production batches (with/without 0.0035% Ce). Characterization via SEM/EDS, automatic inclusion analysis, and Factsage thermodynamic simulations revealed that Ce addition reduced spherical Al-Mg-Ca-O-S inclusions (from 24 to 7 per 2 mm^2; size decreased from 17 μm to 10 μm) while promoting composite inclusions with $AlCeO_3$-Ca(Mn)S cores and Ce-containing Ti(C)N shells. Although square Ti(C)N inclusion numbers remained stable, their average size increased from 8 μm to 11 μm. Ce addition eliminated banded microstructure and refined grains through heterogeneous nucleation (Ce_2O_3 exhibits low misfit of 4.00% with α-Fe). Mechanically, yield strength increased marginally (<5%) with unchanged tensile strength and reducing elongation. However, −20 °C impact toughness decreased by 22%. This duality—beneficial grain refinement versus detrimental coarsening of angular TiN inclusions acting as stress concentrators—provides critical insights for optimizing Ce addition in industrial Ti-bearing high-strength steel BT700L.

Keywords: BT700L beam steel; Ce; TiN; inclusion modification; grain refinement; impact toughness

1. Introduction

With the increasing demand for lightweight materials in the automotive industry, high-strength steels are being widely used in commercial vehicles. BT700L, as a typical high-strength beam steel, is extensively applied in structural components such as frame cross-members and longitudinal beams of heavy-duty vehicles. These components are subjected to complex alternating loads and low-temperature impact conditions during service. However, the control of inclusions in steel has become one of the key factors affecting its mechanical properties, particularly fatigue life and impact toughness. In traditional processes, BT700L steel is mainly modified through aluminum deoxidation and calcium treatment to form low-melting-point calcium aluminate inclusions, thereby reducing their harmful effects on the matrix. Nevertheless, these inclusions may still exhibit issues such as large sizes and uneven distribution during subsequent hot working, making it difficult to completely eliminate their negative impact on toughness [1–3]. Currently, industrially produced BT700L steel typically contains 0.07–0.09% Ti, which enables grain refinement and precipitation strengthening through the formation of TiC and TiN precipitates [4–6]. However, in actual production, large-sized (>10 μm), angular TiN inclusions are easily formed.

Check for updates

Academic Editor: Umberto Prisco

Received: 6 May 2026
Revised: 6 June 2026
Accepted: 8 June 2026
Published: 11 June 2026

Copyright: © 2026 by the authors. Licensee MDPI, Basel, Switzerland. This article is an open access article distributed under the terms and conditions of the Creative Commons Attribution (CC BY) license.

These inclusions have weak bonding with the iron matrix and a significant difference in thermal expansion coefficients, making them prone to becoming microcrack sources under stress, thereby significantly reducing the low-temperature impact toughness and fatigue life of the steel [7,8]. This has become a key technical challenge restricting the safe service of BT700L under harsh conditions. Therefore, exploring new methods to effectively control TiN inclusions holds important engineering significance. Recent studies have increasingly focused on the use of rare earth elements to modify inclusions in high-strength steels [9–12]. However, most of these studies were conducted under laboratory conditions with limited Ti and Ce contents, and systematic industrial-scale investigations on Ce-Ti interaction in BT700L steel remain scarce [13–15].

In recent years, rare earth elements, due to their excellent chemical reactivity and ability to modify inclusions, have garnered increasing attention in steel research. Studies have shown that the addition of trace rare earth elements can significantly refine oxide and sulfide inclusions and can also form rare earth-based composite inclusions. In Ti-bearing steels, the addition of cerium (Ce) leads to the preferential formation of fine and dispersed Ce_2O_3 and $CeAlO_3$ inclusions, which act as heterogeneous nucleation cores for TiN, promoting the precipitation of TiN on their surfaces and forming composite Ce-Al-O(-S-Ca) + TiN inclusions [9–11]. However, the effect of Ce on TiN inclusions in Ti-bearing steels is dual in nature. Studies by Peng Jun et al. [12] showed that an appropriate amount of rare earth elements can refine TiN inclusions and promote their uniform distribution, but excessive rare earth elements may cause TiN inclusions to cluster and grow, increasing the number of large inclusions and negatively affecting the steel's properties. Preliminary experiments in our lab also showed that adding Ce could refine the microstructure without significantly affecting the mechanical properties. Therefore, it is of great theoretical and engineering significance to investigate the evolution of TiN inclusions and their effects on mechanical properties in industrial BT700L steel, which contains specific Ti content (0.078–0.082%). Compared with previous laboratory studies on Ce-modified Ti-bearing steels [9–12], industrial trials involve more complex solidification paths, higher cooling rates, and interactions with Ca, Mg, and S, which may lead to different inclusion evolution behaviors [16–18]. Thus, industrial-scale validation is urgently needed.

In summary, while rare earth elements have shown promise in modifying inclusions and refining grains in Ti-bearing steels, the literature remains limited in addressing their dual effects—especially the coarsening of angular TiN inclusions—under industrial production conditions [19–21]. Thus, this study focuses on the industrial production of BT700L steel, where the cerium addition (0.0035%) is tested, to investigate its effects on inclusions (especially TiN inclusions), microstructure, and mechanical properties. Combining Factsage thermodynamic calculations and two-dimensional misfit degree analysis, the study explores the mechanisms by which Ce regulates the precipitation and growth of TiN inclusions and clarifies its effects on grain refinement and fracture behavior. The results can provide a theoretical basis for the application of rare earths in Ti-bearing high-strength steels and offer references for optimizing the inclusion control process in BT700L steel and enhancing its overall mechanical properties.

2. Materials and Methods

2.1. Experimental Process

The experimental material was BT700L steel produced by a steel company's plate factory. The experiment was carried out using two consecutive batches of steel. The entire production process was identical for both batches, except for the addition of rare earth elements in Furnace #2. Batch 1, without cerium, was used as the control, while Batch 2, with cerium, was the experimental batch. The production process is described as follows:

The molten iron undergoes deep desulfurization in a KR furnace, followed by primary decarbonization in a converter. The steel temperature upon tapping is ≥1620 °C, and aluminum, silicon, and manganese alloys are added for deoxidation and alloying. Slag formation, deoxidation, desulfurization, and composition adjustment occur in the LF furnace. Titanium iron is added during the RH vacuum treatment process, and calcium treatment is carried out after the vacuum treatment, with a soft-blow time of ≥15 min. In the cerium-added batch, 30 kg of rare earth alloy (30% Ce content) was added at the final stage of the RH vacuum treatment.

The continuous casting process adopted protective pouring measures, with slab cross-sectional dimensions of 1830 × 230 mm^2 and casting speed of 1.1 m/min. The superheat was maintained at 25–26 °C. Chemical compositions of the intermediate ladle samples were analyzed using a direct-reading spectrometer (ARL-4460, Thermo Fisher Scientific Inc., Waltham, MA, USA), and cerium content in the steel was determined using Inductively Coupled Plasma Mass Spectrometry (ICP-MS). The chemical compositions of the two batches are shown in Table 1. After casting, the slabs were rolled at a final rolling temperature of 840 °C, followed by a segmented cooling process, and the steel plates were coiled at 580 °C with a final thickness of 8 mm.

Table 1. Chemical Composition of the Experimental 700L Beam Steel (wt.%).

Sample Number	C	Si	Mn	P	S	Al	Ti	Ca	Ce	T.O	N
1#	0.07	0.07	1.66	0.012	0.001	0.037	0.080	0.0014	0	0.0013	0.0042
2#	0.07	0.06	1.68	0.011	0.002	0.038	0.081	0.0012	0.0035	0.0012	0.0041

2.2. Characterization

Samples were taken from the middle of the width of the hot-rolled steel plates. The samples were processed into cylindrical specimens of 7 mm in diameter for oxygen and nitrogen content analysis using an ON836 analyzer (LECO Corp., St. Joseph, MI, USA). Metallographic samples of 10 × 10 × 8 mm were prepared by grinding and polishing. A Zeiss optical microscope (Oberkochen, Germany) was used to observe the types and sizes of inclusions, and a Sigma 300 field-emission scanning electron microscope (Carl Zeiss AG, Oberkochen, Germany) was used to analyze the inclusion types and compositions. Automatic inclusion analysis was performed using an OTS (Oxford Total Solution) inclusion analysis system integrated with the Sigma 300 SEM. For each sample, 10 random fields of view were examined, with a total analyzed area of 2 mm^2 per field. The number of inclusions was counted per 2 mm^2, and average values with standard deviations were reported. Spherical inclusions were defined as those with an aspect ratio < 1.5, characterized by Al-Mg-Ca-O-S elements; square inclusions were defined as those with an aspect ratio ≥ 1.5 and regular square morphology, characterized by Ti and N (with minor C). The size of spherical inclusions was represented by the equivalent circle diameter, while the size of square Ti(C)N inclusions was represented by the length of the long side. The metallographic samples were etched with a 4% nitric acid-alcohol solution to observe the grain size in the transverse and longitudinal directions of the steel plates. Charpy impact tests were performed using an NI750 impact testing machine (NCS Testing Technology Co., Ltd., Beijing, China) to evaluate impact toughness. FactSage software (version 8.2) was used to calculate inclusion formation, utilizing the FactPS, FToxid, FSstel databases, and a custom CESO database. A dissolved oxygen content of 0.0003 wt.% (3 ppm) was adopted as free [O] based on industrial practice for Al-killed steels, following the approach validated in previous studies [13,14].

3. Results and Discussion

3.1. Influence of Ce on Inclusions

Figure 1 shows the metallographic observations of inclusions in the steel after the addition of cerium. It can be seen that Sample 1 (without Ce) contains large spherical inclusions (Al_2O_3-MnS) and small, dispersed square-shaped inclusions (Ti(C)N). In comparison, in Sample 2 (with Ce), the number of large spherical inclusions decreased, and larger fine, dispersed inclusions appeared, with spherical inclusions at the core and square inclusions at the periphery.

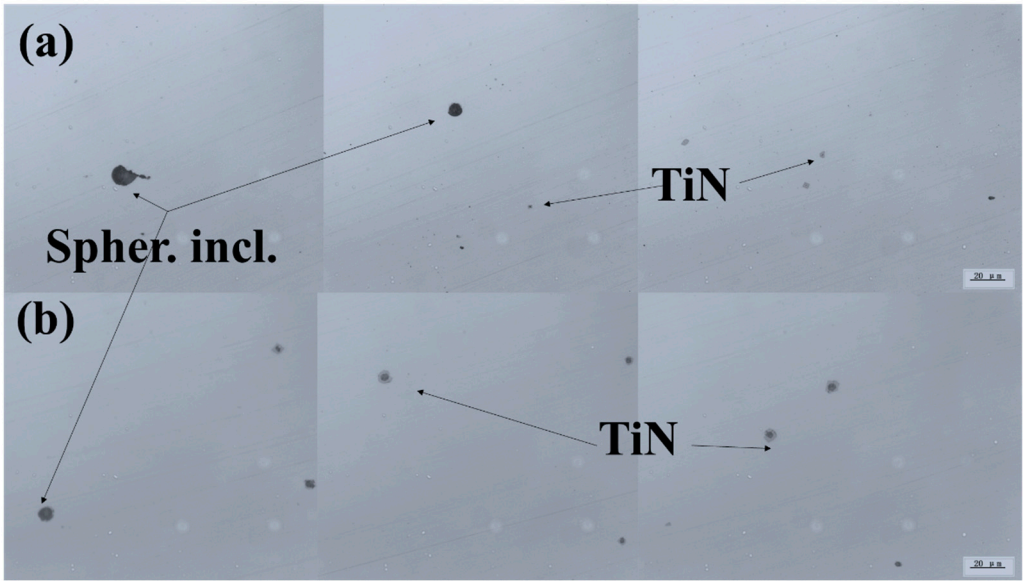


Figure 1. Sample 1 (**a**), Sample 2 (**b**).

Figure 2 presents the statistical data on the number and size of inclusions in 2 mm^2 areas for Sample 1 and Sample 2. Compared to Sample 1, Sample 2 showed a reduction in the number of spherical inclusions from 24 to 7, with the size of spherical inclusions decreasing from 17 μm to 10 μm. The number of square inclusions remained approximately the same at around 75, but the average size of square inclusions increased from 8 μm to 11 μm.

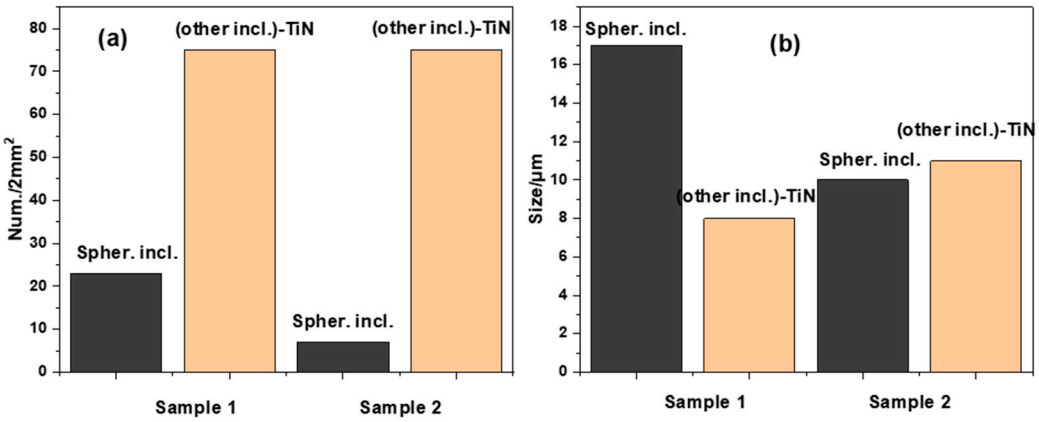


Figure 2. The number (**a**) and size (**b**) of inclusions.

Figure 3 shows typical scanning electron microscope (SEM) images and energy dispersive spectroscopy (EDS) spectra of inclusions in Sample 1 and Sample 2. In Sample 1, spherical inclusions are mainly composed of Al-Mg-O-S-Ca elements, with a small amount

of Ti-N elements at the edges. In Sample 2, square inclusions are mainly composed of Ti-N, with an Al-Mg-O-S-Ca-Mn core and a Ti-N-Ce shell at the outer layer.

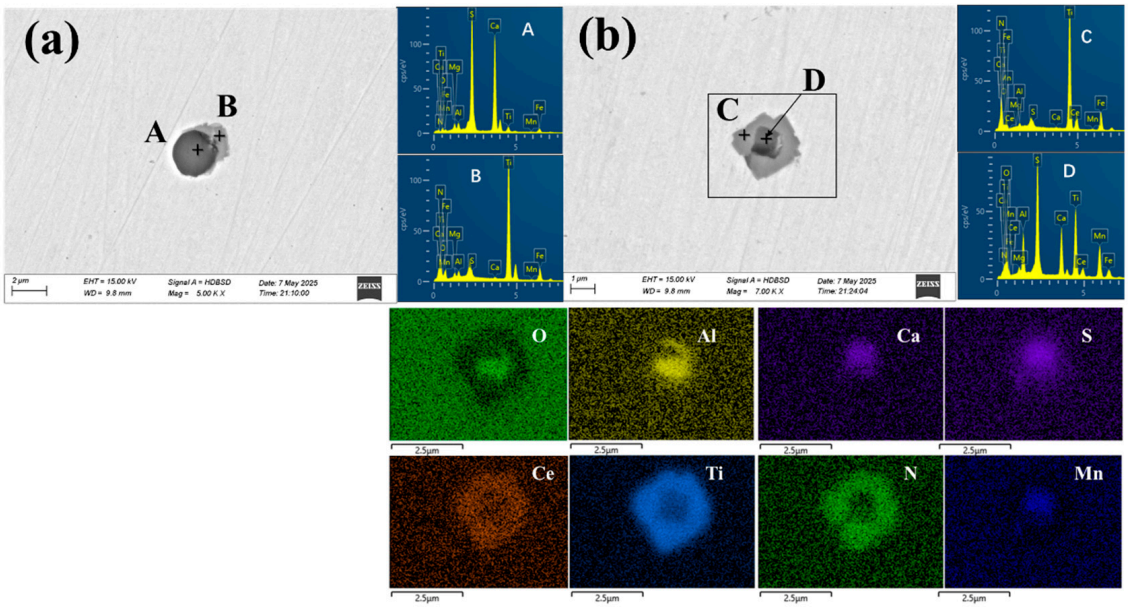


Figure 3. Sample 1: (**a**), Sample 2: (**b**).

During the cooling and solidification of the molten steel, inclusions in both samples also undergo changes. Factsage 8.2 software was used to calculate the changes in inclusion formation. The composition conditions were based on the average values for each component, as shown in Table 1. It is important to note that in the calculations, the dissolved oxygen in the molten steel was chosen, where 0.0003% O represents the measured value of free [O] in industrial aluminum-killed steel production. This is because the Al_2O_3 inclusions formed are difficult to decompose. The selection of free [O] aligns better with the actual observed results, which has also been confirmed in previous studies [13,14]. The results from 1600 °C to 1300 °C are shown in Figure 4. Sample 1 predominantly formed Ca-Al-O inclusions and Ca(Mn)S inclusions in Figure 4a, while Sample 2 formed Ce_2O_3, $AlCeO_3$, and Ca(Mn)S inclusions in Figure 4b. Figure 4c illustrates the precipitation behavior of carbonitrides (Ti(C)N) during the solidification process from 1600°C to 1300°C for both Sample 1 and Sample 2. Since the Ti, C, and N compositions of the two samples are nearly identical (as shown in Table 1), only one representative plot is presented. It can be observed form Figure 4c that TiN begins to precipitate first after solidification, followed by TiC at lower temperatures, and they coexist in the form of solid-solution Ti(C)N.

Through the thermodynamic calculations of inclusion formation and observational analysis, it can be concluded that the inclusions in Sample 1 are mainly spherical composite inclusions (Ca-Al-O inclusions, Ca(Mn)S inclusions, and some adsorbed TiN inclusions) and small, dispersed square Ti(C)N inclusions. In Sample 2, the inclusions mainly consisted of fewer spherical composite inclusions ($AlCeO_3$, Ca(Mn)S, and outer Ti(C)N) and larger, dispersed square composite inclusions with an $AlCeO_3$-Ca(Mn)S core and a Ce-containing Ti(C)N shell.

The change in inclusions after the addition of rare earth elements involves two main issues. The first issue is the reduction in large spherical inclusions, which is primarily caused by the decrease in large spherical composite inclusions after the addition of cerium (Ce). The main reason for this is that the binding force between Ce and oxygen (O) in the molten steel is higher than that of aluminum (Al), leading to a stronger driving force. The greater the driving force, the smaller the nucleation radius. Furthermore, after adding Ce,

the residual Ce and O in the molten steel are almost negligible, which effectively reduces the subsequent growth of inclusions. This is the primary reason for the refinement of large inclusions.

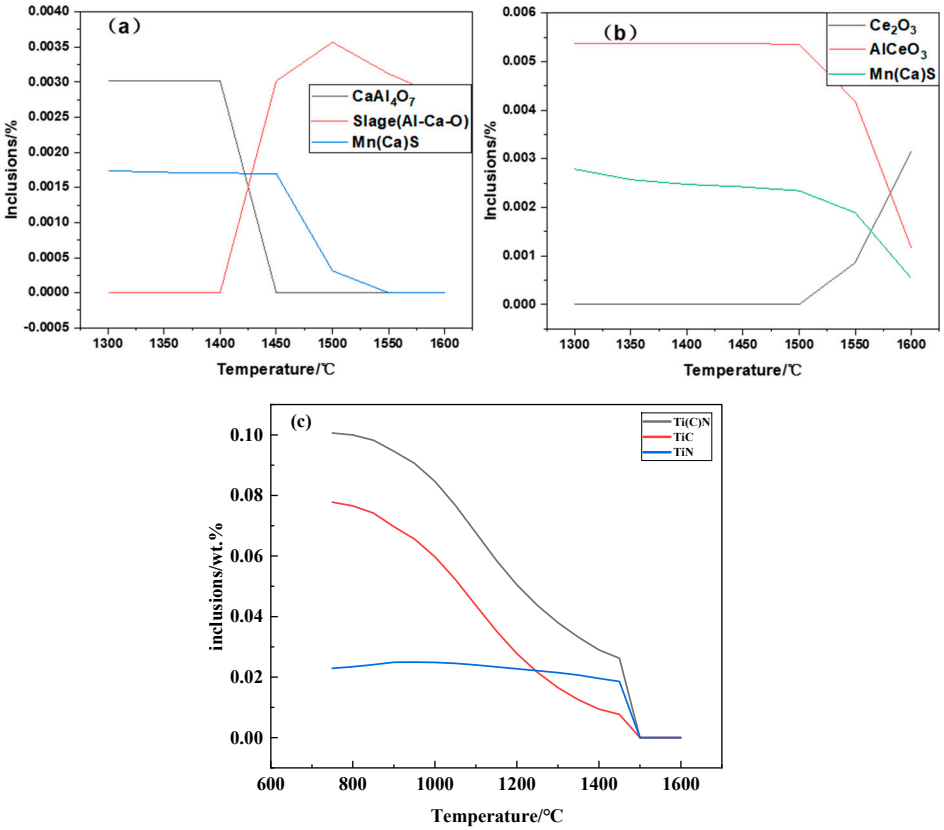


Figure 4. The changes in inclusions from 1600 °C to 1300 °C: Sample 1 (**a**), Sample 2 (**b**), Sample 1 and Sample 2 for Ti(C)N (**c**).

The second issue is the increase in the size of square Ti(C)N inclusions. The main reason for this is that Ti(C)N tends to nucleate on the fine, dispersed Ce-based inclusions formed, resulting in the formation of larger, dispersed square composite inclusions. This phenomenon is consistent with the findings of Zhang et al. [11] in laboratory Ti-bearing steels, where Ce promoted TiN nucleation on $CeAlO_3$ cores. However, unlike their observation of refined TiN at higher Ce levels (0.0055–0.0120%), the present industrial trial with lower Ce content (0.0035%) led to coarsening of Ti(C)N from 8 μm to 11 μm. This discrepancy suggests a critical dependence of TiN size on Ce concentration, cooling rate, and competitive precipitation with Ca/Mg-bearing inclusions [22,23].

It is worth noting a discrepancy between the experimental observations and FactSage thermodynamic predictions. While FactSage calculations (Figure 4b) predict the formation of Ce_2O_3, $AlCeO_3$, and Ca(Mn)S as stable inclusions under equilibrium conditions, SEM/EDS analysis (Figure 3b) reveals Al-Mg-Ca-O-S cores with Ce-containing Ti(C)N shells. This mismatch can be attributed to non-equilibrium solidification kinetics and the low Ce content (0.0035%) in the industrial process. During rapid cooling (approximately 10–100 K/s in continuous casting), kinetic limitations hinder the complete transformation of pre-existing Al-Mg-Ca-O inclusions to Ce-based oxides, leaving Al-Mg-Ca-O-S remnants in the core. Additionally, the limited Ce availability preferentially segregates to the inclusion surface, forming a Ce-containing shell rather than fully replacing the core constituents. Therefore, the observed core–shell structure represents a kinetically frozen intermediate

state, while FactSage predictions represent the thermodynamic endpoint that may not be fully achieved under industrial solidification conditions.

3.2. Influence of Ce on the Microstructure

As shown in Figure 5, Sample 1 (without Ce) presents a banded microstructure with alternating ferrite and pearlite, whereas in Sample 2 (with Ce), the banded structure disappears, and the grains are refined. According to the quantitative analysis conducted using the intercept method in accordance with the GB/T6394-2017 standard[24], the average grain size number increased from 12.71 in Sample 1 to 13.40 in Sample 2, corresponding to a refinement of approximately 0.69 grain size grades. The main influence of Ce on the microstructure is attributed to the formation of inclusions. Therefore, from the perspective of inclusions, the effect of Ce on the microstructure was analyzed in terms of the influence of inclusions on grain nucleation. The two-dimensional misfit degree method was used to calculate the nucleation effectiveness of inclusions on the grain refinement process, as shown in Tables 2 and 3.

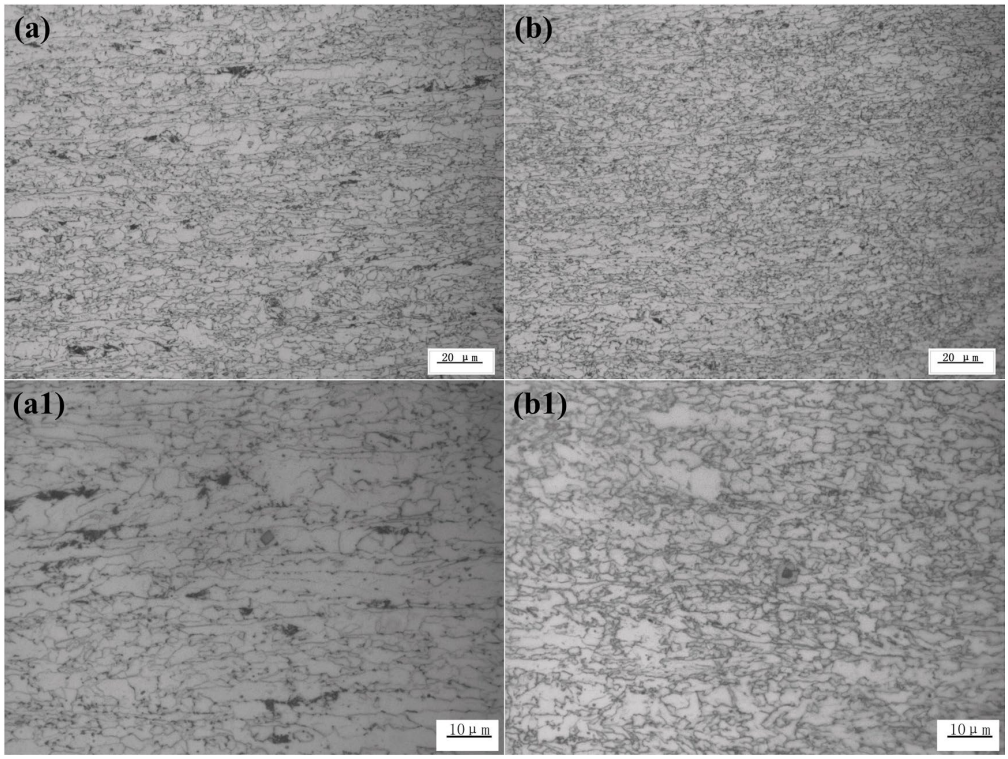


Figure 5. The microstructural morphology of the samples: Sample 1 (**a**) and (**a1**), Sample (**b**) and (**b1**).

Table 2. The relevant crystal structure parameters of inclusions, α-Fe and γ-Fe.

Inclusion	Crystallographic System	Lattice Constant/nm			Source from
		a	b	c	ICDD-PDF-2009
TiN	cube	0.3975			PDF-card: 00-038-1420
Ce_2O_3	hexagonal	0.3891		0.6063	PDF-Card: 00-023-1048
$CeAlO_3$	cube	0.3807			PDF-Card: 00-055-0890
α-Fe	cube	0.2866			PDF-Card: 00-006-0696
γ-Fe	cube	0.3578 * [16]			

Note: * $a_{\gamma\text{-Fe}} = 0.36486 \times [1 + 21.1 \times 10^{-6}(T\text{-}912)$, T: °C.

Table 3. Results of calculation of the lattice misfit degrees.

Case	$[hkl]_s$	$[hkl]_n$	$d[hkl]_s$/nm	$d[hkl]_n$/nm	θ_1/°	$d[hkl]_s \cdot \cos\theta_1$/nm	δ
(001)TiN//(001) α-Fe	[110] α-Fe	[010] TiN	0.4052	0.424	0	0.4052	4.41%
	[1-10] α-Fe	[100] TiN	0.4052	0.424	0	0.4052	
	[100] α-Fe	[110] TiN	0.2866	0.299	0	0.2866	
(001)TiN//(001) γ-Fe	[010] γ-Fe	[010] TiN	0.3578	0.424	0	0.3578	15.61%
	[100] γ-Fe	[100] TiN	0.3578	0.424	0	0.3578	
	[110] γ-Fe	[110] TiN	0.5059	0.5995	0	0.5059	
(0001) Ce_2O_3//(111) α-Fe	[110] α-Fe	[1210] Ce_2O_3	0.4053	0.3891	0	0.3891	4.00%
	[121] α-Fe	[1100] Ce_2O_3	0.7020	0.6739	0	0.6739	
	[011] α-Fe	[2110] Ce_2O_3	0.4053	0.3891	0	0.3891	
(0001) Ce_2O_3//(111) γ-Fe	[100] γ-Fe	[1210] Ce2O3	0.3578	0.3891	15	0.3758	6.28%
	[011] γ-Fe	[1100] Ce_2O_3	0.6197	0.6739	0	0.6739	
	[001] γ-Fe	[2110] Ce_2O_3	0.3578	0.3891	15	0.3758	
(111) $CeAlO_3$//(100) α-Fe	[010] α-Fe	[110] $CeAlO_3$	0.2866	0.2687	15	0.2768	14.93%
	[011] α-Fe	[121] $CeAlO_3$	0.4053	0.2687	0	0.4053	
	[001] α-Fe	[011] $CeAlO_3$	0.2866	0.2687	15	0.2768	

During the liquid phase, Ce_2O_3 inclusions form, which can hinder grain growth in Figures 5 and 6. The Ce_2O_3 inclusions exhibit low misfit degrees with bcc-Fe (α-Fe) and fcc-Fe γ-Fe), with values of 4.00% and 6.28%, respectively, thus promoting heterogeneous nucleation of the grains, contributing to grain refinement. The misfit calculations follow Bramfitt's classical theory using low-index planes/directions, representing theoretical optimal nucleation conditions rather than orientation-specific TEM measurements. According to Bramfitt's criterion, Ce_2O_3 (4.00% with α-Fe) and TiN (4.41% with α-Fe) both qualify as "high-efficiency" nucleation sites (δ < 6%), indicating strong thermodynamic potential for ferrite nucleation. The calculated misfit values provide a thermodynamic assessment; the actual grain refinement effectiveness is also influenced by kinetic factors including inclusion size, distribution, and cooling rate. The predicted refinement is experimentally verified by the increased grain size number (from 12.71 to 13.40) and disappearance of banded structure in the Ce-containing steel (Figure 5), demonstrating qualitative consistency between the misfit calculations and observed microstructural evolution. Additionally, the TiN inclusions in the final composite $AlCeO_3$-TiN inclusions have a low misfit degree (4.41%) with bcc-Fe, further promoting grain refinement. In contrast, in the samples without Ce, no effective second-phase particles were formed during the solidification process, and as a result, grain refinement was limited. TiN exhibits a low misfit of 6.28% with Ce_2O_3 on the (0001)Ce_2O_3//(111)TiN interface and 7.84% with $CeAlO_3$ on the (111)$CeAlO_3$//(111)TiN interface (calculated values based on crystallographic data from Table 2). Both values are below the critical threshold of 12% for effective heterogeneous nucleation, indicating that Ce_2O_3 and $CeAlO_3$ can serve as potent nucleation sites for TiN. This low misfit provides a thermodynamic driving force for TiN to preferentially nucleate on pre-formed Ce-based oxide cores rather than homogeneously in the steel matrix.

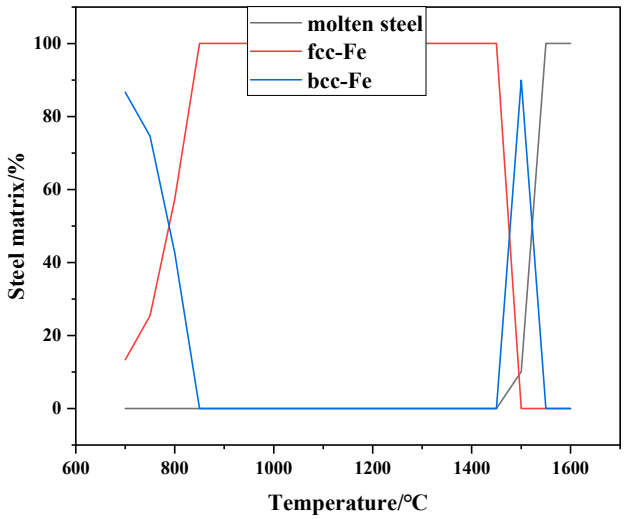


Figure 6. The phase transformation process of the steel matrix.

The misfit degree between inclusions and α-Fe/γ-Fe nucleation effectiveness is calculated using the two-dimensional misfit method [15].

$$\delta = \frac{|\, d_{[uvw]_s} - d_{[uvw]_n} \cdot \cos\theta \,|}{d_{[uvw]_s}} \quad (1)$$

where $(hkl)_s$ represents the low index planes of α-Fe, $[uvw]_s$ represents the low index direction of $(hkl)_s$, $(hkl)_n$ represents the low index planes of Ce-based inclusions, $[uvw]_n$ represents the low index direction of $(hkl)_n$, $d[uvw]_s$ and $d[uvw]_n$ are the interatomic spacings of $[uvw]_s$ and $[uvw]_n$, θ is the angle between $[uvw]_n$ and $[uvw]_s$.

The dual effect of Ce on TiN inclusions—refinement versus coarsening—can be explained by a competition between nucleation promotion and Ostwald ripening. Ce facilitates the formation of fine Ce-bearing oxide cores that act as heterogeneous nucleation sites for TiN, leading to a higher number density of fine TiN precipitates initially. However, during subsequent solidification and cooling, these composite inclusions are prone to Ostwald ripening, where larger particles grow at the expense of smaller ones to minimize interfacial energy. The slight solubility of Ce in TiN may further enhance atomic diffusion, accelerating coarsening. Specifically, Ce segregation at TiN interfaces plays a critical role in this coarsening process. As a surface-active element, Ce preferentially segregates to TiN/matrix and TiN/oxide interfaces, reducing the interfacial energy. While this lowered interfacial energy facilitates heterogeneous nucleation of TiN on Ce-bearing oxides (beneficial effect), it also reduces the thermodynamic barrier for Ostwald ripening by decreasing the energy penalty associated with interface migration. Concurrently, the lattice distortion induced by the slight solubility of Ce in TiN increases vacancy concentration or creates diffusion channels, thereby enhancing the effective diffusion coefficients of Ti and N between TiN particles. The combination of reduced interfacial energy and accelerated atomic diffusion kinetics shifts the balance from nucleation-dominated refinement to ripening-dominated coarsening under the low Ce addition condition (0.0035%).

3.3. Influence of Ce on the Mechanical Properties

Figure 7a shows the yield strength, tensile strength, and elongation properties of Sample 1 and Sample 2. As seen in the figure, the addition of Ce results in a slight increase in yield strength, while tensile strength remains unchanged. The elongation also remains largely unchanged, with changes all within 5%, indicating that Ce addition has little effect on the tensile properties. Figure 7b presents the impact toughness at −20 °C for Sample

1 and Sample 2. It can be seen that the addition of Ce decreases the impact toughness by approximately 22%, indicating that cerium addition has a detrimental effect on the low-temperature impact toughness.

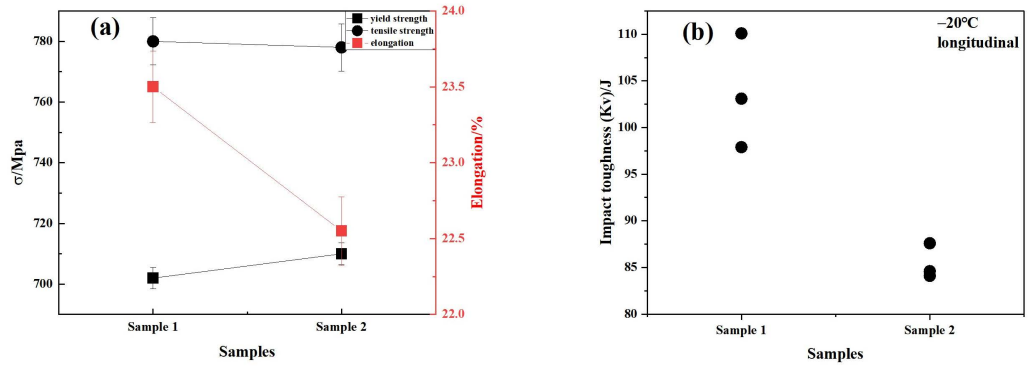


Figure 7. Mechanical Properties: (**a**) Tensile properties; (**b**) Impact toughness.

Figure 8 shows the fracture morphology of the impact specimens for both samples. Both samples exhibit ductile fracture characteristics with the presence of dimples. In Sample 1, spherical inclusions (approximately 8 μm) are found in the dimples, while in Sample 2, angular TiN inclusions (approximately 4 μm) are observed, consistent with the previous observations of inclusions.

To further elucidate the detrimental role of angular Ti(C)N inclusions on toughness, high-magnification SEM observations were conducted on impact fracture surfaces and polished cross-sections of Ce-containing steel (Sample 2). As shown in Figure 8b,b1, large angular Ti(C)N inclusions (approximately 4–11 μm in size) with sharp edges and corners were frequently observed at the bottom of dimples or on cleavage facets. These angular inclusions act as stress concentrators due to their poor coherency with the ferrite matrix and significant mismatch in thermal expansion coefficients. Under impact loading, local plastic deformation is constrained around these hard and brittle inclusions, leading to early microvoid formation and subsequent crack initiation. Quantitative inclusion analysis (Figure 2) revealed that the average size of square Ti(C)N inclusions increased from 8 μm in Ce-free steel to 11 μm in Ce-containing steel, with a population of inclusions exceeding 10 μm in size. This coarsening effect, combined with their angular morphology, explains the 22% reduction in impact toughness at −20 °C, as larger angular inclusions are more likely to exceed a critical size for brittle fracture initiation. Therefore, while Ce addition refines grains and modifies oxide inclusions, the concurrent coarsening of angular Ti(C)N inclusions poses a significant threat to low-temperature toughness.

From the observations above, it can be seen that the addition of Ce refines the grains and generally improves yield strength, tensile strength, elongation, and impact toughness. However, the experimental results did not show a significant improvement in these properties. In fact, the impact toughness decreased, which can be attributed to the changes in inclusion characteristics. The primary reason for this reduction in toughness is that the addition of Ce promotes the formation of larger, dispersed composite $AlCeO_3$-TiN inclusions, with TiN inclusions becoming larger. Large, angular TiN inclusions are detrimental to toughness because they are hard and brittle, with weak bonding to the iron matrix and a large difference in thermal expansion coefficients [17,18]. Under stress (especially during tensile loading), these inclusions become stress concentrators, leading to early crack initiation and subsequent fracture. For yield strength, the effect is relatively small, as it mainly depends on lattice resistance, grain boundaries, and dislocation motion. Large inclusions have limited interference during the elastic deformation stage and do not significantly affect the overall stress distribution. However, the influence on tensile strength and

plasticity is more substantial, as TiN inclusions, being hard and brittle, weaken the interface between the inclusion and the matrix, leading to early failure through microvoids [17,19,20]. Regarding impact toughness, at low temperatures, large TiN inclusions can act as the source of brittle fracture initiation. This leads to a reduction in low-temperature impact toughness. According to the Griffith criterion, the critical fracture stress is inversely proportional to the square root of the defect size. The increase in TiN size from 8 μm to 11 μm corresponds to a ~37.5% increase in defect size, significantly lowering the energy required for crack initiation. Similar detrimental effects of angular TiN inclusions on low-temperature toughness have been reported in Ti-microalloyed steels [17,18,25]. Yan et al. [17] demonstrated that TiN inclusions larger than 10 μm act as preferential cleavage initiation sites under impact loading. Our findings align with this threshold, further confirming that Ce-induced TiN coarsening outweighs the beneficial grain refinement in terms of toughness degradation.

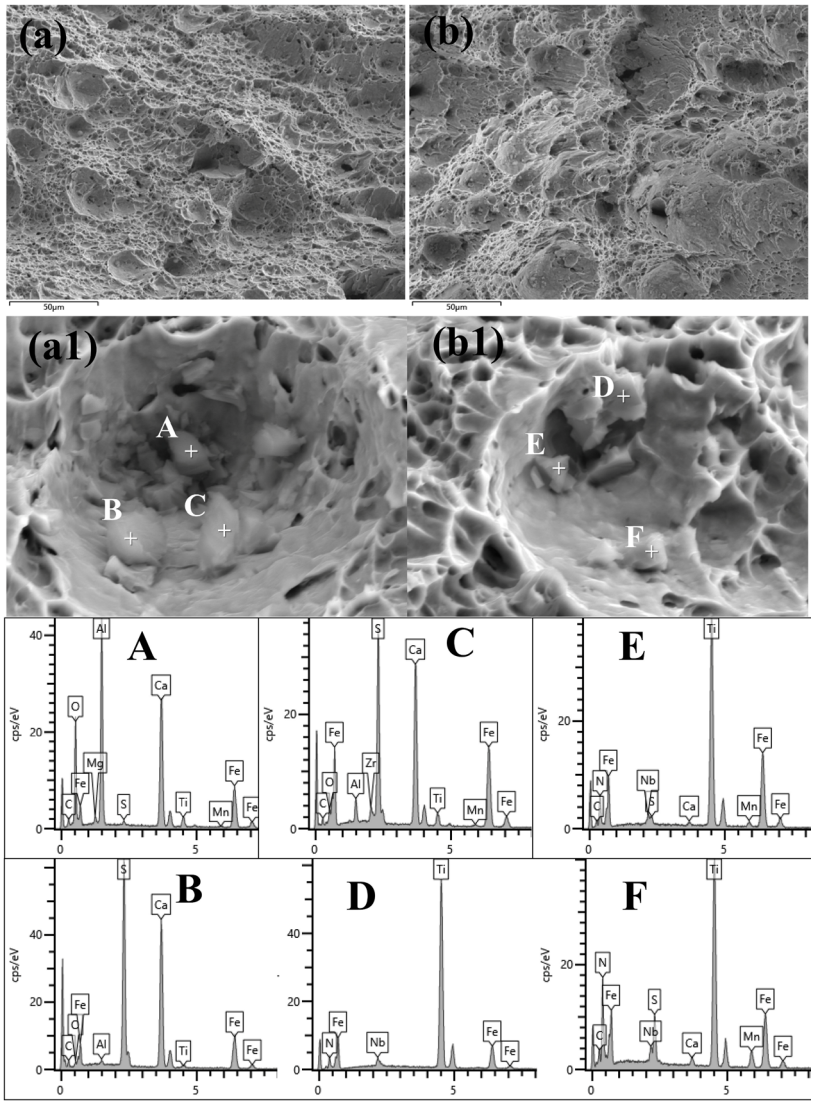


Figure 8. Impact Fracture Morphology: Sample 1 (**a**,**a1**); Sample 2 (**b**,**b1**).

The effect of Ce on TiN inclusions and impact toughness observed in this industrial study differs from our previous laboratory findings. In the laboratory study, a higher Ce addition (0.0055–0.0120%) promoted the formation of finer TiN-based inclusions (down to approximately 1.7 μm), achieved grain refinement, and did not significantly degrade impact toughness, as the embrittlement effect of dispersed TiN nearly offset the toughening effect brought about by grain refinement. In contrast, in this industrial trial, a lower Ce

addition (0.0035%) led to coarsening of Ti(C)N inclusions (from 8 μm to 11 μm) due to Ostwald ripening and complex interactions with other alloying elements (e.g., Ca, Mg, S). Consequently, the toughening effect from grain refinement was overshadowed by the detrimental effect of large, angular Ti(C)N inclusions acting as crack initiation sites, resulting in a 22% reduction in impact toughness at −20 °C. This discrepancy highlights the critical roles of Ce content, competitive precipitation of inclusions, and cooling conditions in determining, and suggests that there exists an optimal Ce addition range in Ti-bearing steels produced industrially to balance grain refinement and toughness.

To further understand why the detrimental effect on TiN outweighs the beneficial grain refinement, a quantitative comparison is necessary. According to the Griffith criterion for brittle fracture, the critical fracture stress is inversely proportional to the square root of the defect size. The increase in TiN inclusion size from 8 μm to 11 μm represents a ~37.5% increase in defect size, leading to a significant reduction in critical fracture stress. In contrast, the grain size number increase from 12.71 to 13.40 corresponds to only a modest reduction in ferrite grain size. The beneficial contribution from grain refinement is insufficient to compensate for the detrimental effect caused by TiN coarsening.

Based on the experimental observations, a critical TiN size threshold of approximately 10 μm is identified. In the Ce-containing steel (Sample 2), where TiN inclusions exceed this threshold with an average size of 11 μm and exhibit angular morphology (aspect ratio $\geq$ 1.5), a 22% reduction in impact toughness is observed. In contrast, in the Ce-free steel (Sample 1), where TiN inclusions are smaller (8 μm) and fewer angular features are present, no such severe toughness degradation occurs. Therefore, the combination of size >10 μm and angular morphology (aspect ratio $\geq$ 1.5) defines the critical condition under which TiN inclusions become detrimental to low-temperature impact toughness in BT700L steel. This threshold provides a practical guideline for industrial production: TiN inclusions should be controlled to remain below 10 μm in size, or their angular morphology should be suppressed, to avoid significant toughness loss when adding Ce.

4. Conclusions

(1) The addition of cerium significantly altered the types, morphology, and distribution of inclusions in BT700L steel. In the sample without Ce (Sample 1), two types of inclusions were primarily present: spherical Al-Mg-Ca-O-S composite inclusions (average size of 17 μm) and small, dispersed square Ti(C)N inclusions (average size of 8 μm). After the addition of 0.0035% Ce (Sample 2), the number of spherical composite inclusions decreased by about 70%, and their average size was refined to 10 μm. The number of square Ti(C)N inclusions remained roughly the same, but the average size increased to 11 μm, and a composite structure formed, with $AlCeO_3$-Ca(Mn)S as the core and a Ce-containing Ti(C)N shell on the outside.

(2) Two-dimensional misfit degree calculations showed that Ce_2O_3 inclusions had a misfit degree of 4.00% with α-Fe and 6.28% with γ-Fe, both lower than the critical value for effective heterogeneous nucleation (12%), indicating that these inclusions could effectively promote heterogeneous nucleation of ferrite and facilitate grain refinement. The misfit degree between $AlCeO_3$ and α-Fe was higher (14.93%), but the composite $AlCeO_3$-TiN inclusions, due to the low misfit degree between TiN and α-Fe (4.41%), still contributed to grain refinement. Microscopic observations confirmed that the addition of Ce led to the disappearance of the original banded structure and significant grain refinement.

(3) Mechanical property testing showed that the addition of cerium had a minor effect on the tensile properties of BT700L steel. Yield strength increased slightly, while tensile strength and elongation remained mostly unchanged. However, the low-temperature

impact toughness decreased by about 22%, indicating a negative effect on impact toughness.

(4) Ce exhibits a dual effect in Ti-bearing high-strength steel. On the beneficial side, Ce refines oxide inclusions (reducing the size of spherical inclusions from 17 μm to 10 μm) and promotes grain refinement through heterogeneous nucleation on Ce_2O_3. On the detrimental side, Ce induces coarsening of angular Ti(C)N inclusions (from 8 μm to 11 μm). The size increase and angular morphology of Ti(C)N are more critical to toughness than the beneficial effects of grain refinement or oxide inclusion refinement, because large (>10 μm), angular TiN inclusions act as preferential stress concentration points under low-temperature impact loading, promoting early microcrack initiation and unstable crack propagation.

In summary, Ce addition of 0.0035% in industrial BT700L steel is insufficient to achieve the desired balance between strength and toughness. Although this addition level refines oxides and grains, it also promotes detrimental coarsening of angular TiN inclusions, leading to a net loss in impact toughness. Under the current Ce addition level, it is necessary to optimize the cooling conditions and the Ti/N ratio to inhibit Ostwald ripening of Ti(C)N inclusions. In Ti-bearing high-strength steel, precise control of the Ce addition level is crucial for balancing grain refinement, inclusion modification, and low-temperature toughness.

Author Contributions: Methodology, C.S. and X.Z.; validation, J.H. and C.Y.; formal analysis, P.L. and C.Y.; investigation, C.S. and P.L.; writing—original draft preparation, C.S. and X.Z.; writing—review and editing, X.Z. and J.Y.; project administration, J.H. and J.Y. All authors have read and agreed to the published version of the manuscript.

Funding: This research was funded by the Advanced Materials-National Science and Technology Major Project (No.2024ZD0606400), Scientific Research Special Project for First-Class Disciplines of Education Department of Inner Mongolia Autonomous Region (No.YLXKZX-NKD-001), and Basic Scientific Research Business Expenses of Colleges and Universities of Inner Mongolia Autonomous Region (No. 2024CXPT001).

Data Availability Statement: The original contributions presented in the study are included in the article, further inquiries can be directed to the corresponding authors.

Conflicts of Interest: Authors Chao Shi, Xiaofeng Zhang and Jianzhong He were employed by the company Technical Center of Inner Mongolia Baotou Steel Union Co., Ltd. The remaining authors declare that the research was conducted in the absence of any commercial or financial relationships that could be construed as a potential conflict of interest.

References

1. Li, M.; Wu, H.; Sun, Y. Effect of the inclusion features on mechanical properties of steel. *Ironmak. Steelmak.* **2022**, *49*, 405–411. [CrossRef]
2. Dekkers, R.; Blanpain, B.; Wollants, P.; Haers, F.; Vercruyssen, C.; Gommers, B. Non-metallic inclusions in aluminium killed steels. *Ironmak. Steelmak.* **2003**, *29*, 437–444. [CrossRef]
3. Zhao, D.; Li, H.; Cui, Y.; Yang, J. Control of Inclusion Composition in Calcium Treated Aluminum Killed Steels. *ISIJ Int.* **2016**, *56*, 1181–1187. [CrossRef]
4. Yang, L.; Li, Y.; Xue, Z.L.; Cheng, C.G. Influence of Ti(C,N) precipitates on austenite growth of micro-alloyed steel during continuous casting. *China Foundry* **2017**, *14*, 421–428. [CrossRef]
5. Hao, J.; Wang, C.; Duan, H.; Yan, Z.; Yuan, G.; Wang, G. TiN-containing high-heat-input welding steels: Optimizing Ti/N ratio and precipitation temperature for enhanced low-temperature impact toughness in coarse-grained heat-affected zones. *J. Mater. Res. Technol.* **2025**, *36*, 9641–9651. [CrossRef]
6. Liu, T.; Chen, D.; He, W.; Long, M.; Gui, L.; Duan, H.; Cao, J. Study on the formation and control of tin inclusion in mushy zone for high Ti microalloyed steel. In *Proceedings of the TMS Annual Meeting & Exhibition*; Springer: Berlin/Heidelberg, Germany, 2018; pp. 605–615. [CrossRef]

7. Wu, X.; Zuo, X.; Zhao, W.; Wang, Z. Mechanism of TiN Fracture During the Tensile Process of NM500 Wear-Resistant Steel. *Acta Metall. Sin.* **2020**, *56*, 129–136. [CrossRef]
8. Yan, W.; Shan, Y.; Yang, K. Effect of TiN inclusions on the impact toughness of low-carbon microalloyed steels. *Metall. Mater. Trans. A* **2006**, *37*, 2147–2158. [CrossRef]
9. Liu, S.; Yang, F.; Liu, L.; Wang, J.; Peng, J.; Zhang, F.; An, S. Effects of rare earth Ce on TiN inclusion modifications in 20CrMnTi steel under deoxygenation conditions of Si–Ca–Ba alloy. *J. Mater. Res. Technol.* **2024**, *30*, 223–230. [CrossRef]
10. He, F.; Peng, J.; Zhang, F.; Wang, Y.; Chang, H. Experimental and first-principles calculation of TiN growth mechanism on CeAlO3 surface in steel. *J. Iron Steel Res. Int.* **2024**, *31*, 452–463. [CrossRef]
11. Zhang, X.; Xu, Y.; Yang, C.; Song, X.; Zhi, J.; An, S. Effect of Ce addition on inclusions, microstructure and impact toughness in Ti-bearing low-carbon Al-killed steel. *J. Mater. Res. Technol.* **2025**, *37*, 4631–4638. [CrossRef]
12. Zhang, Y.; Peng, J.; Zhang, F.; Chang, H.; Liu, L.; Yu, X. Effect of rare earth cerium on precipitation of TiC and Ti(C, N) in titanium microalloyed steel. *J. Iron Steel Res. Int.* **2022**, *34*, 1160–1168. [CrossRef]
13. Zhang, X.; Zhi, J.; Song, X.; Diao, W.; Lu, B.; An, S. Influence of cerium on impact toughness, tensile properties and inclusion of industrial Al-killed steel Q355B. *J. Mater. Res. Technol.* **2024**, *32*, 1118–1126. [CrossRef]
14. Zhang, X.; Zhi, J.; Song, X.; Li, Z.; An, S. Mechanism of cerium-based inclusion formation and influence on impact toughness in industrial Al-killed steel. *Ironmak. Steelmak.* **2024**, *51*, 33–42. [CrossRef]
15. Bramfitt, B.L. Planar lattice disregistry theory and its application on heterogistry nuclei of metal. *Met. Trans.* **1970**, *1*, 1987–1995. [CrossRef]
16. Yong, Q. *Secondary Phases in Steels*; Metallurgical Industry Press: Beijing, China, 2006.
17. Yan, W.; Shan, Y.; Yang, K. Influence of TiN inclusions on the cleavage fracture behavior of low-carbon microalloyed steels. *Metall. Mater. Trans. A* **2007**, *38*, 1211–1222. [CrossRef]
18. Fairchild, D.P.; Howden, D.G.; Clark, W.A.T. *Cleavage Initiation in Ti Microalloyed Steels*; ASM International: Materials Park, OH, USA, 1995; p. 310.
19. Zhu, Y.; Lu, Y.M.; Huang, C.W.; Liang, Y.L. The effect of TiN inclusions on the fracture mechanism of 20CrMnTi steel with lath martensite. *Mater. Res. Express* **2020**, *7*, 16. [CrossRef]
20. León-García Orlando, O.; Petrov, R.; Kestens, L.A.I. Void initiation at TiN precipitates in IF steels during tensile deformation. *Mater. Sci. Eng. A* **2010**, *527*, 4202–4209. [CrossRef]
21. Gui, L.; Long, M.; Zhang, H.; Chen, D.; Liu, S.; Wang, Q.; Duan, H. Study on the precipitation and coarsening of TiN inclusions in Ti-microalloyed steel by a modified coupling model. *J. Mater. Res. Technol.* **2020**, *9*, 5499–5514. [CrossRef]
22. Shu, Q.; Visuri, V.V.; Alatarvas, T.; Fabritius, T. A Kinetic Model for Precipitation of TiN Inclusions from Both Homogeneous and Heterogeneous Nucleation During Solidification of Steel. *Metall. Matefromrans. B* **2022**, *53*, 2321–2333. [CrossRef]
23. Wang, J. Study on the Effect and Mechanism of Rare Earth Ce on the Modification of TiN Inclusions in 20CrMnTi Gear Steel. Master's Thesis, Inner Mongolia University of Science and Technology, Baotou, China, 2023.
24. *GB/T 6394-2017*; Determination of Average Grain Size of Metal. Standardization Administration of China: Beijing, China, 2017.
25. Liu, T.; Long, M.; Chen, D.; Duan, H.; Gui, L.; Yu, S.; Cao, J.; Chen, H.; Fan, H. Effect of coarse TiN inclusions and microstructure on impact toughness fluctuation in Ti micro-alloyed steel. *J. Iron Steel Res. Int.* **2018**, *25*, 1043–1053. [CrossRef]

Disclaimer/Publisher's Note: The statements, opinions and data contained in all publications are solely those of the individual author(s) and contributor(s) and not of MDPI and/or the editor(s). MDPI and/or the editor(s) disclaim responsibility for any injury to people or property resulting from any ideas, methods, instructions or products referred to in the content.